Evaluation of the corrosion resistance of plasma nitrided austenitic stainless steel

Daniel Mareci[a], Sorin Iacob Strugaru[b], Corneliu Munteanu[b], Georgiana Bolat[a], Ricardo M. Souto[c]

[a]Faculty of Chemical Engineering and Environmental Protection, "Gheorghe Asachi" Technical University of Iasi, Iasi, Romania

[b]Faculty of Mechanical Engineering, "Gheorghe Asachi" Technical University of Iasi, Iasi, Romania

[c]Department of Chemistry, University of La Laguna, La Laguna, Tenerife, Spain

Plasma nitriding at 500 °C for 14 h was applied to austenitic 304 stainless steel for surface hardening. The effect of surface treatment on the corrosion resistance of the material was investigated in naturally-aerated 0.5 M NaCl solution for 30 days using linear potentiodynamic polarization and electrochemical impedance spectroscopy methods. Both as-cast and plasma nitrided stainless steel samples underwent spontaneous passivation, though the nitrided sample exhibited more positive zero current potential, higher breakdown potential, and lower anodic current densities than the as-cast material. Impedance spectra were interpreted in terms of a duplex passive film, corrosion resistance mainly arising from a thin inner compact layer, whereas the outer layer was more porous and less sealing. Capacitive behaviour and high corrosion resistance were observed in the low and medium frequency ranges for the nitrided samples.

Keywords: Plasma nitriding; 304 austenitic stainless steel; Corrosion; SEM; Electrochemical characterization.

1. Introduction

Austenitic stainless steels have good corrosion resistance, but their low hardness and low wear resistance limit their use whenever surface hardness is required [1]. It is known that nitriding is an efficient way to improve the mechanical and tribological properties of the material surfaces [2–6]. In addition to mechanical changes, surface modification by nitriding also affects the corrosion behaviour of a steel due to the diffusion of nitrogen into the alloy surface [2, 3, 5, 7–12], including austenitic stainless steels [13–16]. Yet there are conflicting reports as to whether the effect of nitrogen implantation on the corrosion characteristics of the material is beneficial or deleterious [15, 17, 18]. The use of plasma-nitriding temperatures as low as 350 °C does not promote degradation in the corrosion resistance of stainless steel [13, 19–23]. Nitriding at a temperature around 500 °C can produce a thick nitrided layer on the austenitic stainless steel surface, which significantly improves the surface hardness and wear properties [24]. However, chromium nitride (CrN) formed during nitriding has been regarded as a crucial factor in affecting the corrosion resistance of a nitrided austenitic stainless steel [25].

The corrosion destruction of a metal or alloy from its reaction with the environment is mainly an electrochemical oxidation process that usually produces soluble metal ions and other metallic oxides. Since corrosion is an electrochemical process it requires an electrolyte or current-carrying medium between different parts of the corrosion cell. In chloride-containing aqueous environments, there are two competitive processes operating simultaneously in the system, namely the chloride ion activity –which tends to destroy the passive film– and the dissolved oxygen –which promotes formation and repair of the passive film on metallic materials. In this framework, electrochemical methods are an efficient and convincing tool for the analysis of the corrosion behaviour of metals or alloys [26, 27].

This paper concentrates on the evaluation of the corrosion resistance of plasma nitrided austenitic stainless steel exposed to aerated 0.5 M NaCl aqueous solution at 25 °C, bearing in mind that the chloride ion is present in many corrosion situations. In the present work, austenitic stainless steel was plasma nitrided at 500 °C following the methodologies generally used in this technique. Electrochemical impedance spectroscopy (EIS) measurements were performed at the open-circuit potential, and they were interpreted by fitting to an electrical equivalent circuit (EC) describing the physicochemical properties of the protective surface layer formed on the material. Film morphology and type of the corrosive attack were characterized using scanning electron

(SEM) and optical (OM) microscopies, whereas the phase constituents of the surface layer were analyzed by means of X-ray diffraction (XRD) analysis.

2. Materials and methods

2.1. Sample preparation

Austenitic stainless steel AISI 304 was used. Samples about 10 mm thick were cut from bar of 30 mm diameter. Samples were wet-polished with 400, 600, 1000, and 2500 grit metallographic abrasive papers, final polishing was done with 1 μm alumina suspension. The samples were degreased with ethyl alcohol followed by ultrasonic cleaning with deionized water. The nitrided samples were prepared at the Grupo T.T.N. S.P.A. Nitrurazioni Cementazioni Bonifiche Ricotture Tempra Sottovuoto Sale Induzione (Nerviano, Italy) in a DC glow discharge plasma nitriding unit for 14 hours at a temperature of 500 °C. The treatment gas was 20 % N_2 + 80 % H_2 (at.%).

2.2. Corrosion testing

The investigation of the corrosion characteristics of both as-cast and plasma nitrided austenitic stainless steel was carried out in 0.5 M NaCl aqueous solution with *pH* = 6.9, maintained at 25 ± 1 ^{o}C. The test specimens were placed in a glass corrosion flow cell kit (C145/170, Radiometer Analytical, Lyon, France), which was filled with saline solution [28]. Test specimens were embedded in a polytetrafluoroethylene (PTFE) holder specifically designed to connect to a rotating disc electrode (type EDI 101T; Radiometer Analytical). A polymeric resin was used to ensure a tight seal between the specimen and the PTFE holder, to avoid crevice corrosion [29]. A saturated calomel electrode (SCE) used as the reference electrode, and a platinum coil as the counter electrode completed the electrochemical cell.

Electrochemical measurements were performed using a potentiostat manufactured by PAR (Model PARSTAT 4000, Princeton Applied Research, Oak Ridge, TN, USA). The instrument was controlled by a personal computer and specific software (*VersaStudio*, Princeton Applied Research). For both as-cast and nitrided samples, specimens with a nominal surface area of 7.1 cm^2 were immersed into stagnant and naturally aerated electrolyte for 2 h in order to attain a stable open-circuit potential measurement. The evolution of the open-circuit potential values from immersion until stabilization was monitored against the SCE reference electrode.

Potentiodynamic polarization tests were conducted at a scan rate of 0.5 mV s^{-1} in the potential range from –800 to +1000 mV vs. SCE. Using an automatic data acquisition system, the linear potentiodynamic polarization curves were plotted and both the corrosion current density (i_{cor}) and the zero current potential (E_{cor}) were estimated. In order to evaluate the stability of the passive state, passivation current density (i_{pas}) and breakdown potential (E_{bd}) were also determined from the linear potentiodynamic polarization curves. EIS studies were conducted in the frequency range of 10 kHz to 10 mHz with a 10 mV amplitude around the open circuit potential. The relevant corrosion parameters were extracted from the fit of a relevant equivalent circuit (EC) to the EIS data using the ZSimpWin version 3.22 software (Princeton Applied Research). The typical guidelines for the selection of the best-fit EC were followed, namely a minimum number of circuit elements were employed, the χ^2 error was suitably low ($\chi^2 < 10^{-4}$), and the error associated with each element was below 5 %.

2.3. Material characterization

The cross-sectional microstructure of the nitrided samples was examined using OM with a LEICA DMI5000 M (Leica Microsystems, Wetzlar, Germany) inverted metallographic microscope equipped with a dedicated digital camera connected to a personal computer and analyzed with the Leica Application Suite software program. The phase constituents of the nitrided austenitic stainless steel were analyzed by means of XRD analysis with an X'Pert PRO MRD (PANalytical, Eindhoven, The Netherlands) diffractometer using Cu K_α radiation. The XRD patterns were scanned in the 30° ≤ 2-Theta ≤ 60° range at a rate of 1.8° min^{-1}.

The type of corrosion attack experienced by the materials during linear polarization experiments was characterized by means of SEM using a VEGA II LSH (Tescan, Brno, Czech Republic) microscope operated at 30 kV accelerating voltage.

3. Results and discussion

Figure 1 shows the OM cross-sectional view of plasma nitrided austenitic stainless steel produced at 500 °C. In this figure, the light side corresponds to metal (M), while the dark side is the polymeric resin (P). The micrograph of the nitrided sample displays the austenitic matrix and, on top of it, a thin nitrided layer. The thin dark layer was probably formed during the nitriding

process due to the diffusion of atmospheric carbon to the interface between the transformed layer and the substrate [30, 31].

The phase constituents in the nitrided surface were analyzed with XRD using Cu K_α radiation. Figure 2 indicates that the 500 °C nitrided surface consisted mainly of CrN which gave much higher diffraction intensity than the austenite phase of the steel.

The corrosion characteristics of these materials were first investigated using a standard potentiodynamic polarization technique and next by means of electrochemical impedance spectroscopy (EIS) in aerated 0.5 M NaCl aqueous solution, at approximately neutral *pH*. The measurements were made in static conditions, maintaining the solution at rest, to simulate the stagnant conditions of the corrosive medium which are common in practice [32]. Prior to electrochemical testing, samples were left unbiased in the test solution for 2 hours for stabilization while monitoring the evolution of their open circuit potential (E_{oc}) values. The open circuit potential (E_{oc}) of a metal varies as a function of time but stabilizes at a stationary value after a period of immersion. Upon immersion, the corresponding E_{oc} values shifted rapidly towards more positive potential values, as observed in Fig. 3. After ca. 20 min, the rate of variation of E_{oc} values decayed quite significantly, though monotonously shifting in the positive direction until stabilization at the end of the exposure. The open circuit potential of the non-nitrided sample stabilized at –378 mV vs. SCE, whereas the nitrided sample adopted a more positive potential at –295 mV vs. SCE in the test solution. Neither sample exhibited potential drops associated with the surface activation during 120 min exposure in the test medium. This kind of behaviour strongly suggests that the surface of both samples became more thermodynamically resistant to corrosion in aerated 0.5 M NaCl aqueous solution with pH = 6.9 as result of their exposure.

Figure 4 shows the linear polarization curves of both non-nitrided and plasma nitrided austenitic stainless steel samples. The two materials exhibited similar polarization curves. None of them exhibited a distinctive active–passive transition in the polarization curves following the Tafel region, but they entered directly into a stable passive regime. Two distinct regions can be distinguished in the anodic branches of the polarization curves. In the first region, the dissolution of both samples was under kinetic control, and the anodic current density increased very slowly with potential excursion in the positive direction, characteristic of a passive behaviour. Passive current density (i_{pas}) was determined from the potentiodynamic anodic branch and was taken

approximately at the middle of the passive range. In the second region, the rapid increase in the current value is due to breakdown of the passive film. The susceptibility of an alloy to pitting corrosion in a certain medium can be characterized in terms of the breakdown potential (E_{bd}) relative to the zero-current potential value (E_{cor}) [33, 34]. The potential range situated between E_{cor} and E_{bd} represents the passivity zone in which the corrosion rate is low or even insignificant. As the difference between E_{bd} and E_{cor} becomes smaller, the alloy is expected to become more susceptible to pitting corrosion.

As a result of the nitriding process, the zero-current potential of the non-nitrided austenitic stainless steel (i.e., –507 mV vs. SCE) was shifted towards a more noble value (–372 mV vs. SCE). The increase in the value of E_{cor} can be attributed to enhanced passivation promoted by the presence of N. Similar observations regarding the enhancement of passivation by the presence of N have been already reported [35, 36], and they have been attributed to an inhibiting action by N at the surface. It is also interesting to compare the values of E_{cor} derived from the polarization curves (see Fig. 4) with those of E_{oc} spontaneously attained by the samples (cf. Fig. 3). In both cases the values determined for the E_{cor}, are more negative than those corresponding to $E_{oc.}$ This variation is probably due to partial reduction of the spontaneously formed oxide layer on the surface of the materials while recording the cathodic branch of the polarization curves.

The corrosion current density (i_{cor}) is representative of the degradation degree of the alloy. It is evident from Fig.e 4 that there is a decrease of the anodic current of the nitrided sample with respect to the non-nitrided sample. This demonstrates that the nitrided sample has a greater corrosion resistance than the non-nitrided, and this feature originates the measurement of smaller values for the corrosion current densities. The corrosion current density for the non-nitrided sample is approximately three times bigger than in the case of the nitrided sample, when they were obtained in the same conditions. The surface treated at 500 °C exhibited improved corrosion resistance under the testing conditions, despite precipitation of chromium nitride. The difference in the breakdown potentials of the passive film for each material become readily observed from the inspection of the polarization curves.

Table 1 shows the values of breakdown potential (E_{bd}) together with the differences determined for $E_{bd} - E_{cor}$. The onset of localized corrosion occurs at ca. +130 mV vs. SCE for the non-nitrided sample, as given by its corresponding E_{bd} value, and the passive zone extends over

approximately 600 mV. Analogously, the E_{bd} of the nitrided sample is slightly more positive than +200 mV vs. SCE. These potentials, however, are not specific to a particular alloy and hence do not account for variations in the open-circuit values. Thus, the values of $E_{bd} - E_{cor}$ provide a more reliable measure of the breakdown resistance. An alloy with a particular surface condition may exhibit a low E_{bd} but have a sufficiently negative E_{cor} that the difference between them is bigger. These results (Table 1) show that the nitrided and non-nitrided austenitic stainless steel exhibited a similar susceptibility to pitting corrosion resistance based on this parameter.

Breakdown of the surface layer was confirmed by SEM examination of the retrieved samples after completing the polarization tests. Figure 5A and D show that the corrosion defects on a nitrided surface are smaller in size than those on the non-nitrided sample, and they are less numerous for a given area. Furthermore, the shape of single defects on non-nitrided sample correspond well with the observations of local passive oxide film and nucleation of corroding pits (cf. Fig. 5B and C), whereas for the nitrided sample all the exposed metal within the defect seems to corrode more homogeneously. In the latter, breakdown of the nitride layer, probably originating from pores in the deposit, leads to direct exposure of the underlying metal to the aggressive environment that corrodes at the positively-charged substrate (see Fig. 5 E and F).

Further information regarding the corrosion behavior of metallic materials can be obtained using electrochemical impedance spectroscopy (EIS) [37]. The experimental impedance data measured at the open-circuit potential for both the non-nitrided and the plasma nitrided austenitic stainless steel sample immersed for different periods of time in aerated 0.5 M NaCl aqueous solution, at 25 °C, are presented as Nyquist diagrams in Fig. 6. These plots show that the impedance of the materials decrease with the elapse of time, this feature being more pronounced for the non-nitrided material. All the spectra exhibit a capacitive loop (open arc). The diameter of the open arc provides an estimate of the polarization resistance. The decrease in diameter indicates a decrease in corrosion resistance.

Bode plots of the two materials immersed for different periods of time in aerated 0.5 M NaCl aqueous solution are shown in Fig. 7. The advantage of the Bode plot is that the data for all measured frequencies are shown and that a wide range of impedance values can be displayed. The frequency dependence of the phase angle indicates the number of time constants present in the system and can be used to determine the values of the parameters in the equivalent circuit. Two peaks were observed in the Bode-phase plots determined for the plasma nitrided stainless

steel, whereas only one is observed for the non-nitrided steel. This indicates the involvement of two-time constant at open circuit potential for the nitrided austenitic stainless steels sample immersed in aerated 0.5 M NaCl aqueous solution. Rather high impedance values (in the order of 10^5 Ω cm^2) were found in the medium to low frequencies for the nitrided austenitic stainless steels sample supporting that it presents corrosion resistance in the corrosion medium used.

The impedance modulus ($|Z|$) of nitrided austenitic stainless steels sample slowly decreases with the time of sample immersion. All the spectra show that in the higher frequency region, $\log|Z|$ tends to become constant. This is a typical response for the resistive behaviour and corresponds to the solution resistance, R_{sol}. In the medium frequency range, a linear relationship between $\log|Z|$ and $\log f$ is observed in all cases, though with different slopes (always less than –1), whereas the maxima in the phase angle plots are smaller than –90°, indicating that the passive films were not completely capacitive.

For the interpretation of the electrochemical behaviour of a system from EIS spectra, an appropriate physical model of the electrochemical reactions occurring on the electrodes is necessary. The electrochemical system may be represented by an equivalent circuit (EC). In the case of the non-nitrided stainless steel, the spectra could be satisfactorily simulated using the simplified Randles' circuit shown in Fig. 8A, which assumes that the corrosion of the passive material is hindered by an oxide film that acts as a barrier-type layer. The occurrence of a second overlapping wave in the phase shift response of the plasma nitrided material indicates that the spectra cannot be explained by the simple equivalent circuit based on a single parallel combination of a resistance and a constant phase element of Fig. 8A. Therefore, fitting of the impedance was done with the EC depicted in Fig. 8B using a series combination of the solution resistance, R_{sol} (around 75 Ω), with two RQ parallel combinations: R_{sol} (R_1Q_1) (R_2Q_2). This has been proposed to give the electrical representation of two-layer surface films consisting of a barrier-type compact inner layer and a relatively porous outer layer [38–40]. Very good agreement between the simulated and experimental data was obtained. The values of the impedance parameters determined from the fits are presented in Tables 2 and 3 for the non-nitrided and the nitrided steels, respectively. To satisfactorily fit the spectra, a constant phase element (CPE) was used instead of a pure capacitance because of the non-ideal capacitive response. The impedance representation of CPE is given as:

$$Z_{CPE} = \frac{1}{Y_0 (j\omega)^n} \quad (1)$$

where ω is the angular frequency and Y_0 is a constant, and the value of the exponent n indicates the deviation from ideal capacitive behaviour (e.g., when n = 1). In general, the CPE is given as both the capacitance C, expressed in s^n S, and the factor n. The values of exponent were always greater than 0.8, which may indicate a rather smooth surface of the nitrided layer.

The parameters R_1 and Q_1 account for the reactions at the nitrided layer/solution interface and determine the impedance behaviour in the high frequency range of the spectrum. The constant phase element Q_1 represents the double layer pseudo-capacitance of the nitrided layer, as shown by the high value of the n_1 exponent [41]. Therefore, the parameters R_2 and Q_2 describe the properties of the nitrided layer. As immersion time increases from 1 to 30 days, the resistance (R_2) of the nitrided layer decreases slowly from 5.8×10^5 Ω cm^2 to 4.5×10^5 Ω cm^2. However, the values of R_2 are about 10^2 times bigger than those of R_1 at all exposures, thus revealing that nitrided layer provides most of the corrosion protection to the material. The nitrided austenitic stainless steels samples are still highly resistant to corrosion after 30 days immersed in aerated 0.5 M NaCl aqueous solution [42]. The long term performance of the nitrided samples in the test solution is then superior to that of the non-nitrided material. Therefore, the nitriding procedure at 500 °C produced a surface with improved corrosion resistance under the testing conditions, regardless of the chromium nitride precipitation.

4. Conclusions

Very low corrosion current densities (~1 μA cm^{-2}) and passive current densities (~3 μA cm^{-2}) were obtained from the potentiodynamic polarization curves for nitrided austenitic stainless steel sample. The nitrided sample showed more positive zero current (E_{cor}) and breakdown (E_{bd}) potentials than the non-treated material.

The improvement in corrosion resistance was attributed to the formation of a layer containing chromium nitride on the surface of the austenitic stainless steel. However, the protective layers formed on the surface of both non-nitrided and nitrided austenitic stainless steel samples are prone to localized breakdown in chloride-containing solutions as characterized by the measurement of a pitting corrosion potential.

The EIS spectra of the nitrided austenitic stainless steel samples in aerated 0.5 M NaCl aqueous solution exhibited two-time constants; the first accounts for the properties of the reactions at the nitrided layer/solution interfaces, and the second for the nitrided layer. The EIS tests confirm that nitrided austenitic stainless steel exhibit passivity after 30 days immersion in 0.5 M NaCl aqueous solution, at open circuit potential.

The experimental linear polarization curves, EIS diagrams, and the equivalent circuit parameters have shown that the nitrided austenitic stainless steel sample in aerated 0.5 M NaCl aqueous solution presents high electrochemical corrosion resistance.

References

[1] G. Bregliozzi, S.I.-U. Ahmed, A. Di Schino, J.M. Kenny, H. Haefke: Tribol. Lett. 17 (2004) 697.

[2] J.K. Hirvonen, C.A. Carosella, R.A. Kant, I. Singer, R. Vardiman, B.B. Rath: Thin Solid Films 63 (1979) 5.

[3] D.-C. Wen: Surf. Coat. Technol. 204 (2009) 511.

[4] J. Yang, Y. Liu, Z. Ye, D. Yang, S. He: Tribol. Lett. 40 (2010) 139.

[5] C. Nouveau, P. Steyer, K.R.M. Rao, D. Lagadrillere: Surf. Coat. Technol. 205 (2011) 4514.

[6] L.F. Zagonel, J. Bettini, R.L.O. Basso, P. Paredez, H. Pinto, C.M. Lepienski, F. Alvarez: Surf. Coat. Technol. 207 (2012) 72.

[7] J. Flis, J. Mankowski, E. Rolinski: Surf. Eng. 5 (1989) 151.

[8] G.K. Wolf: Surf. Coat. Technol. 83 (1996) 1.

[9] R.M. Souto, H. Alanyali: Corros. Sci. 42 (2000) 2201.

[10] A. Medina-Flores, C. Arganis, P. Santiago, J. Oseguera: Surf. Coat. Technol. 188–189 (2004) 140.

[11] N. Yasavol, F. Mahboubi: Mater. Design 38 (2012) 59.

[12] R.M. Souto, H. Alanyali, R. Rodríguez-Raposo, L. Fernández-Mérida, S. González: Int. J. Electrochem. Sci. 8 (2013) 8530.

[13] M. Samandi, B.A. Shedden, D.I. Smith, G.A. Collins, R. Hutchings, J. Tendys: Surf. Coat. Tech. 59 (1993) 261.

[14] K. Bell, T. Akamatsu: Stainless Steel 2000 - Thermochemical Surface Engineering of Stainless Steel, The Institute of Materials, London (2001).

[15] M.K. Lei, X.M. Zhu: Surf. Coat. Technol. 201 (2007) 6865.

[16] L. Nosei, S. Farina, M. Ávalos, L. Náchez, B.J. Gómez, J. Feugeas: Thin Solid Films 516 (2008) 1044.

[17] W. Ensinger, G.K. Wolf: Mater. Sci. Eng. A 116 (1989) 1.

[18] F.Z. Bouanis, F. Bentiss, M. Traisnel, C. Jama: Electrochim. Acta 54 (2009) 2371.

[19] G.S. Chang, J.H. Son, S.H. Kim, K.H. Chae, C.N. Whang, E. Menthe, K.-T. Rie, Y.P. Lee: Surf. Coat. Tech. 112 (1999) 291.

[20] E. Menthe, K.-T. Rie: Surf. Coat. Tech. 116-119 (1999) 199.

[21] S. Parascandola, W. Möller, D. Williamson: Appl. Phys. Lett. 76 (2000) 2194.

[22] S. Picard, J.B. Memet, R. Sabot, J.L. Grosseau-Poussard, J.-P. Rivière, R. Meilland: Mat. Sci. Eng. 303 (2001) 163.

[23] L.L. Pranevicius, P. Valatkevicius, V. Valincius, C. Templier, J.-P. Rivière, L. Pranevicius: Surf. Coat. Tech. 156 (2002) 219.

[24] C.X. Li, T. Bell: Corros. Sci. 48 (2006) 2036.

[25] X.Y. Li, H. Dong: Mater. Sci. Tech. 19 (2003) 1427.

[26] I.E. Castañeda, J.G. Gonzalez-Rodriguez, J. Colin, M.A. Neri-Flores: J. Solid State Electrochem. 14 (2010) 1145.

[27] S. Nagarajan, V. Raman, N.J. Rajendran: J. Solid State Electrochem. 14 (2010) 1197.

[28] D. Mareci, I. Rusu, R. Chelariu, G. Bolat, C. Munteanu, D. Sutiman, R.M. Souto: Eur. J. Sci. Theol. 9 (2013) 189.

[29] D. Mareci, G. Ciurescu, R. Chelariu, I. Cretescu, D. Sutiman: Environ. Eng. Manage. J. 9 (2010) 81.

[30] M.J. Baldwin, S. Kumar, J.M. Priest, M.P. Fewell, K.E. Prince, K.T. Short: Thin Solid Films 345 (1999) 108.

[31] L.C. Gontijo, R. Machado, S.E. Kuri, L.C. Casteletti, P.A.P. Nascente: Thin Solid Films 515 (2006) 1093.

[32] V. Barranco, S. Feliu Jr., S. Feliu: Corros. Sci. 46 (2004) 2203.

[33] B.E. Wilde, E. Williams: Electrochim. Acta 16 (1971) 1971.

[34] J.R. Scully, R.G. Kelly, in: S.D. Cramer, B.S. Covino Jr. (Eds.), Corrosion: Fundamentals, Testing, and Protection, ASM Handbook 13A, ASM International, Materials Park, OH (2003) 68.

[35] T.M. Muraleedharan, E.I. Meletis: Thin Solid Films 221 (1992) 104.

[36] V. Singh, E.I. Meletis: Surf. Coat. Tech. 201 (2006) 1093.

[37] G. Bolat, D. Mareci, S. Iacoban, N. Cimpoesu, C. Munteanu: J. Spectroscopy (2013) Article ID 714920, 7 pages.

[38] R. Hirayama, S. Haruyama: Corrosion 47 (1991) 952.

[39] F. Mansfeld: Electrochim. Acta 38 (1993) 1891.

[40] J. Pan, D. Thierry, C. Leygraf: Electrochim. Acta 41 (1996) 1143.

[41] M. Meticoš-Huković, Z. Pilić, R. Babić, D. Omanović: Acta Biomater. 2 (2006) 693.

[42] F. Mansfeld: J. Electrochem. Soc. 120 (1973) 515.

Table 1: Corrosion parameters determined from the polarization tests performed in aerated 0.5 M NaCl aqueous solution at 25 ºC.

Sample	E_{cor} (mV vs. SCE)	i_{cor} (μA cm^{-2})	i_{pas} (μA cm^{-2})	E_{bd} (mV vs. SCE)	$E_{bd} - E_{cor}$ (mV)
Non-nitrided	–507	2.3	3.9	+128	635
Nitrided	–372	0.7	3.1	+206	578

Table 2: Values of fitted impedance parameters of non-nitrided austenitic stainless steel as a function of immersion time in aerated 0.5 M NaCl aqueous solution.

Time (day)	Q_1 (μS cm^{-2} s^n)	n_1	R_1 (MΩ cm^2)
1	12	0.87	0.47
2	13	0.87	0.44
7	13	0.86	0.36
14	13	0.86	0.25
21	14	0.86	0.17
30	14	0.85	0.10

Table 3: Values of fitted impedance parameters of nitrided austenitic stainless steel as a function of immersion time in aerated 0.5 M NaCl aqueous solution.

Time (day)	Q_1 (μS cm^{-2} s^n)	n_1	R_1 (kΩ cm^2)	Q_2 (μS cm^{-2} s^n)	n_2	R_2 (MΩ cm^2)
1	21	0.88	4.1	11	0.84	0.58
2	22	0.87	3.7	12	0.83	0.54
7	23	0.86	3.5	12	0.83	0.51
14	23	0.86	3.4	12	0.82	0.48
21	23	0.86	3.1	12	0.82	0.47
30	24	0.86	2.8	13	0.82	0.45

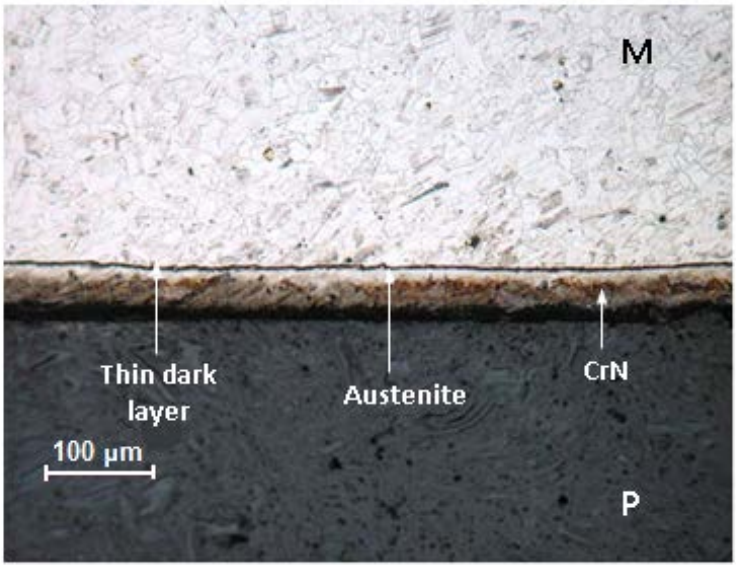

Figure 1: Optical microscopy cross-sectional view of the plasma nitrided austenitic stainless steel produced at 500 °C. (M), metal; (P), polymeric resin.

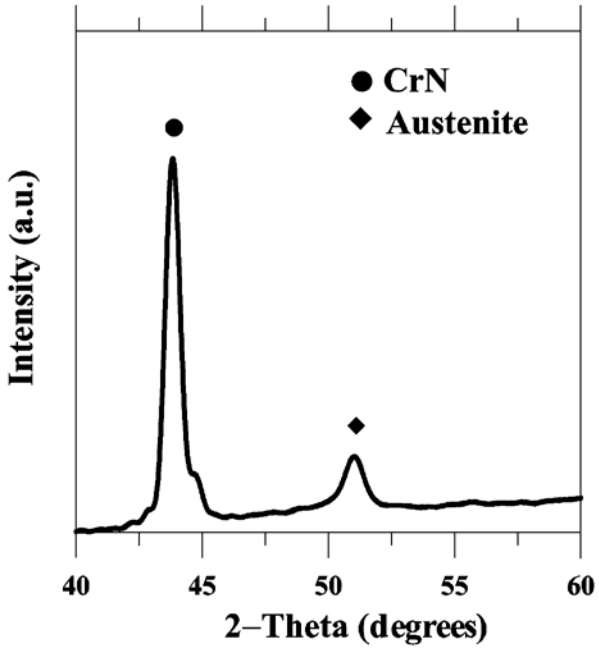

Figure 2: X-ray diffraction pattern of the plasma nitrided austenitic stainless steel.

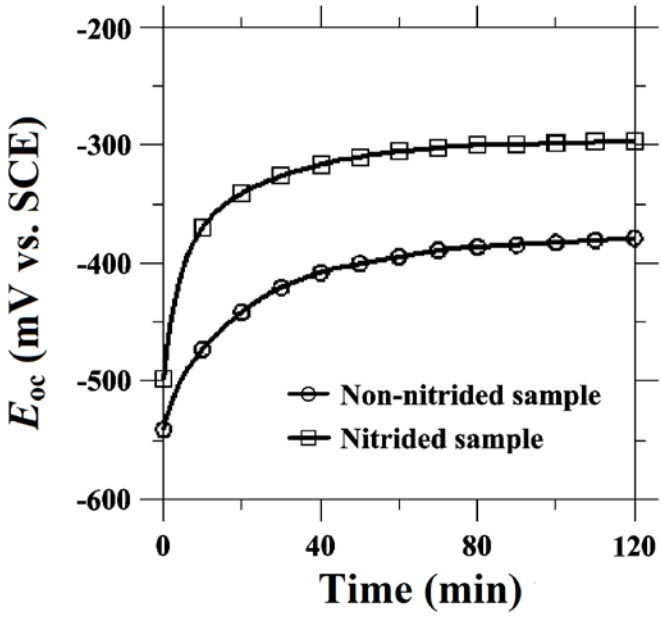

Figure 3: Time evolution of the open circuit potential E_{oc} of non-nitrided and nitrided austenitic stainless steel samples during 2 hours of immersion in aerated 0.5 M NaCl aqueous solution, at 25 °C.

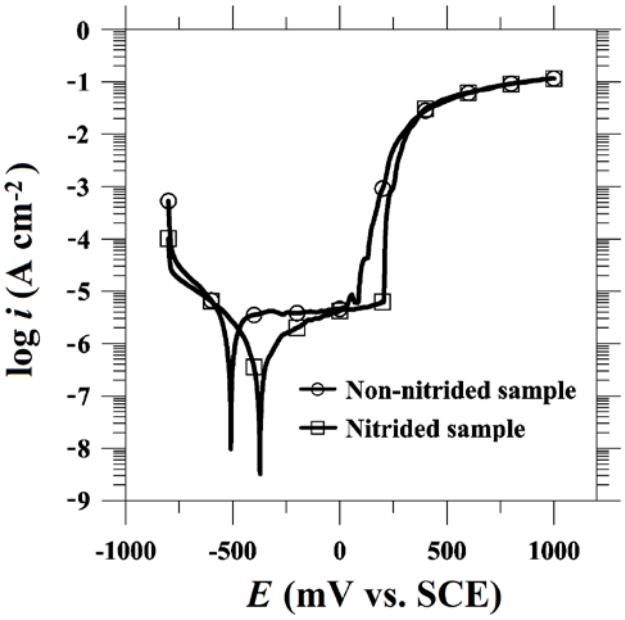

Figure 4: Potentiodynamic polarization curves plotted using semi-logarithmic coordinates of non-nitrided and nitrided austenitic stainless steel samples tested after 2 hours of immersion in aerated 0.5 M NaCl aqueous solution, at 25 °C.

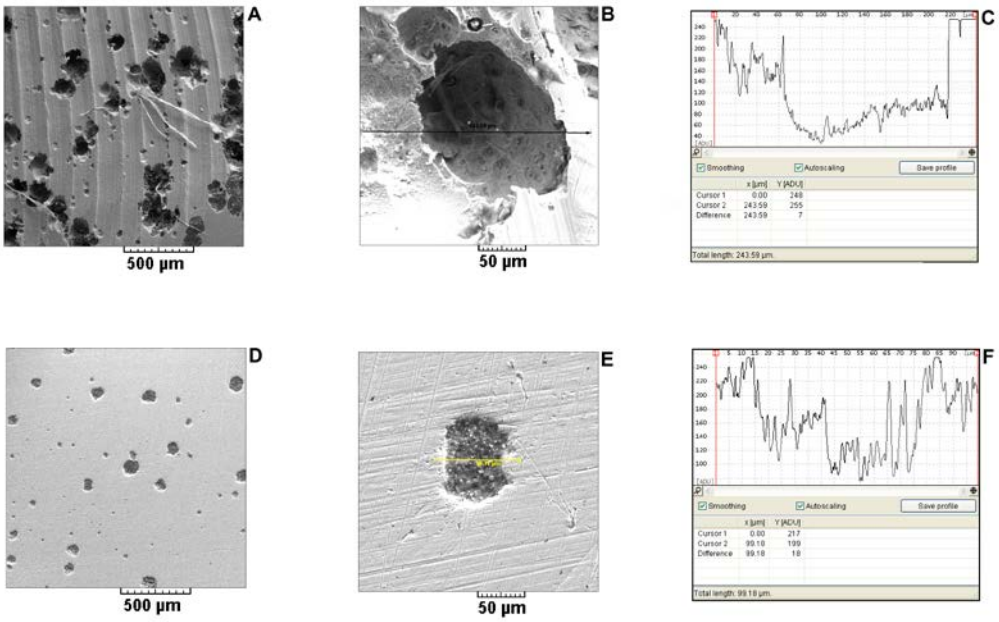

Figure 5: Scanning electron micrographs depicting the surface of retrieved specimens: (A and B) non-nitrided, and (D and E) nitrided. They show the morphology of the corrosive attack experienced in 0.5 M NaCl solution during the measurement of the polarization curves plotted in Fig. 4. The depth profiles of typical single pits taken along a line are given in (C and F).

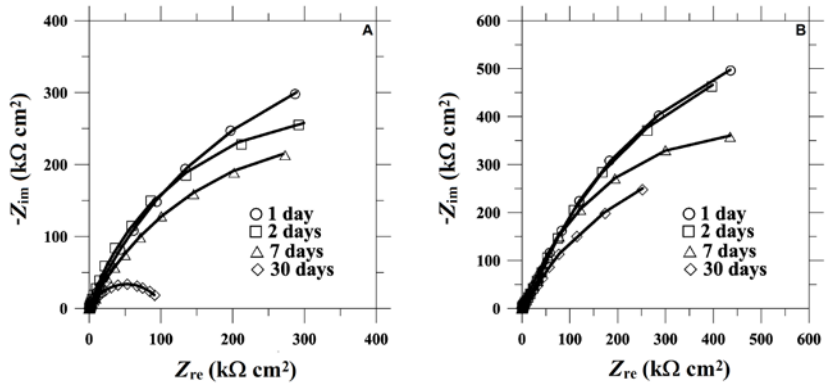

Figure 6: Nyquist plots of the impedance spectra measured for (A) non-nitrided and (B) plasma nitrided austenitic stainless steel as a function of immersion time in 0.5 M NaCl aqueous solution.

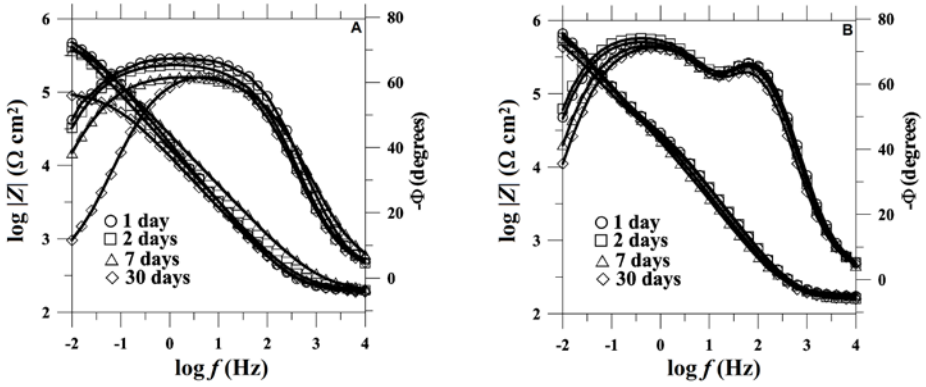

Figure 7: Measured (discrete points) and fitted (solid lines) Bode impedance plots (A) non-nitrided and (B) plasma nitrided austenitic stainless steel as a function of immersion time in 0.5 M NaCl aqueous solution.

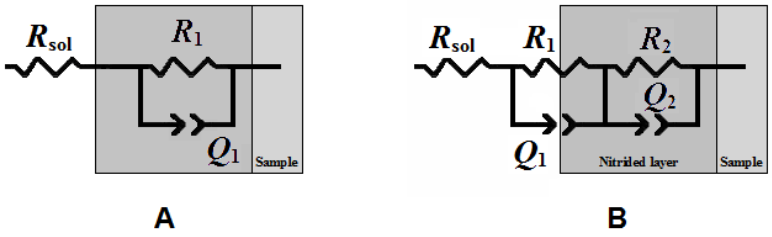

Figure 8: Equivalent circuits (EC) used to fit the impedance data: (A) one-layer model of a barrier-type oxide surface film with one time constant; and (B) two-layer model of an unsealed porous surface film with two time constants.